Actuator Modeling for Attitude Control Using Incremental Nonlinear Dynamic Inversion

F. Binz*, D. Moormann
Institute of Flight System Dynamics, RWTH Aachen University, Wüllnerstr. 7, 52062 Aachen

Abstract

Recently, the concept of Incremental Nonlinear Dynamic Inversion (INDI) has seen an increasing adoption as an attitude control method for a variety of aircraft configurations. The reasons for this are good stability and robustness properties, moderate computation requirements and low requirements on modeling fidelity. While previous work [1] investigated the robust stability properties of INDI, the actual closed-loop performance may degrade severely in the face of model uncertainty. We address this issue by first analyzing the effects of modelling errors on the closed-loop performance by observing the movement of the system poles. Based on this, we analyze the neccessary modeling fidelity and propose simple modeling methods for the usual actuators found on small-scale electric aircraft. Finally, we analyze the actuator models using (flight) test data where possible.

1 Introduction

Incremental Nonlinear Dynamic Inversion (INDI) has been applied to a variety of aicraft including quadrotors, hybrid aircraft (tailsitter, tiltwing) and conventional airplanes [2, 3, 4, 5]. The method was first introduced by NASA [6] and then further developed at TU Delft [2, 3]. At the core of INDI a simple control law given by

$$\delta \mathbf{u} = \mathbf{M}_u^{-1} \cdot J \cdot (\nu - \dot{\Omega}) \tag{1}$$

is used, where ν is the commanded angular acceleration, J is the aircrafts inertia and $\mathbf{M}_u$ describes the actuator effectivity. This paper concentrates on the last term $\mathbf{M}_u$ and the associated neccessary dynamic actuator models. We summarize modeling approaches which have been successfully applied in practice for quadrotors [3], tiltwing [7] or tailsitter [4, 8] aircraft. Since the problem of oscillations frequently arises when applying INDI, we try to gain some insight into this issue by observing the closed-loop system poles. A similar analysis was already done in previous work [1], but concentrates on the stability properties of the closed loop.

*Email address: binz@fsd.rwth-aachen.de

2 Effects of Modeling Uncertainty

The goal of Nonlinear Dynamic Inversion (NDI) is to invert the plant dynamics, so that the resulting closed-loop dynamics are a series of integrators. In principle, the INDI formulation in [3] shares this goal. However, due to the way in which state-derivatives (i. e. angular accelerations) are calculated, the resulting closed-loop dynamics from the commanded anguluar accelerations ν to the actual angular accelerations $\dot{\Omega}$ are the actuator dynamics $A(z)$ in the nominal case. Thus, the design of outer controllers (e.g. angular rate and attitude controllers) is influenced by these actuator dyanmics $A(z)$. One major motivation in using NDI (or INDI), is to simplify the design of outer loop controllers. We thus want to develop an understanding of how well the actuator dynamics and effectivity needs to be known, to still achieve an appropriate outer loop performance.

To analyze this, we assume an INDI-based angular rate controller, as shown in figure 1. For simplicity, we only analyze the single-input single-output case, but expect the results to be transferable in principle to the multiple-input multiple-output case aswell. The parameters of the system consist of the plant parameters – namely the control effectivity M_η, actuator time constant T and actuator delay τ – and the corresponding controller parameters $\hat{M}_u, \hat{T}, \hat{\tau}$. The actuator dynamics are modelled as first-order lags with an optional delay:

$$A(s) = \frac{1}{1+Ts} e^{-\tau s} \tag{2}$$

In the nominal case $\hat{M}_u = M_u, \hat{T} = T$ and $\hat{\tau} = \tau$. To develop an understanding of how uncertainty in the parameters affects the closed loop system, we analyze movement of the system poles when parameters are changed.

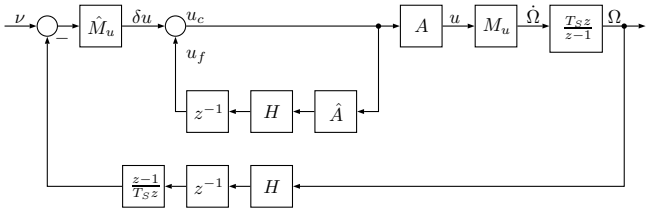

Figure 1: Controller structure

2.1 Poles of the INDI controller

In the nominal case, the closed loop transfer function from the commanded angular accelerations ν to the actual angular

accelerations $\dot{\Omega}$ is equal to the actuator dynamics A. In the non-nominal case additional dynamics appear, because the system poles and zeros don't cancel each other. Since the analytical expression for the closed-loop transfer function in the non-nominal case is somewhat convoluted, we graphically analyze the behaviour of the poles instead. While INDI is an inherently discrete-time control algorithm, we choose to display the poles (and zeros) in the continous-time domain because we are more familiar with this setting.

Figure 2 shows the movement of the poles of the INDI loop, when the control effectivity M_u is incorrect. In the

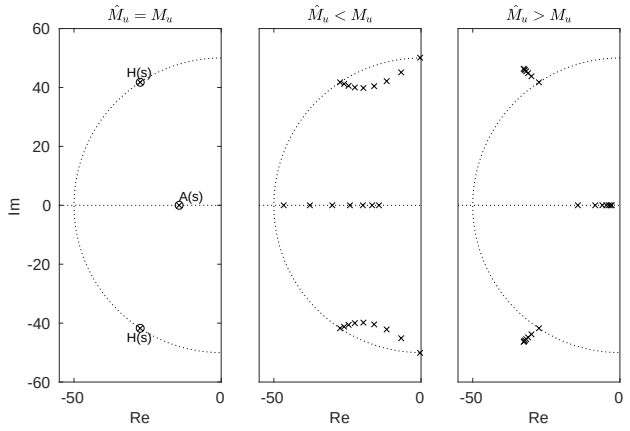

Figure 2: Effect of uncertainty in control effectivity on significant poles of INDI loop, $0.2 < \hat{M}_u/M_u < 4$

nominal case (left), the poles of the filter H are completely cancelled and thus don't influence the closed-loop dynamics. Only the poles of the actuator dynamics A remain. We selected the filter parameters of H as follows:

$$\begin{aligned} H(s) &= \frac{\omega_0^2}{s^2 + 2\zeta\omega_0 s + \omega_0^2} \\ \omega_0 &= 50\,\mathrm{rad\,s^{-1}} \\ \zeta &= 0.55 \end{aligned} \tag{3}$$

For $\hat{M}_u \neq M_u$ the cancellation of the filter poles does not occur. For $\hat{M}_u < M_u$, the poles of the filter H become less damped and start to show as oscillations in the time-domain. The frequency of this oscillation roughly equals the natural frequency ω_0 of the filter H. For $\hat{M}_u > M_u$ the system dynamics basically slows down, because the poles of the assumed actuator dynamics $\hat{A}$ move to the right. For the chosen filter parameters (see (3)), the closed-loop becomes unstable for $\frac{\hat{M}_u}{M_u} < 0.2$, though clearly visible oscillations start to appear at around $\frac{\hat{M}_u}{M_u} < 0.5$. Note, that these margins change when chosing different filter parameters H. In general, a larger damping ratio ζ and a larger natural frequency ω_0 lead to more robustness w.r.t. uncertainty in M_u. At the same time, these filter parameters influence the amount of noise introduced when calculating $\dot{\Omega}$ as well as the disturbance rejection performance [3]. Thus, the filter parameters will be a trade-off between robustness w.r.t. to M_u, performance of disturbance rejection and noise.

Figure 3 shows a similar analysis as before, this time changing the assumed actuator dynamics $\hat{T}$. Here, for $\hat{T} <$

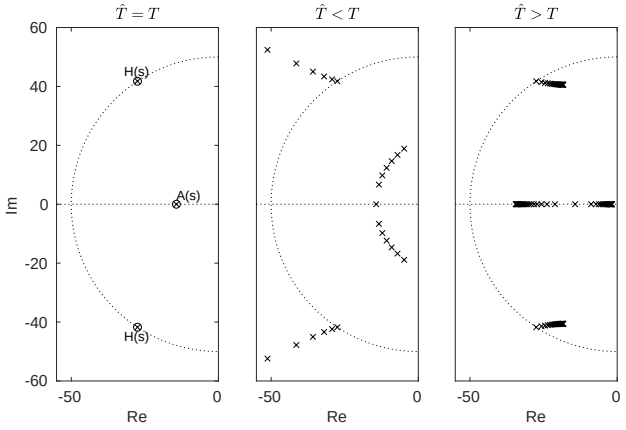

Figure 3: Effect of uncertainty in actuator dynamics on significant poles of INDI loop, $T = 0.07, 0.01 < \hat{T} < 0.14$

T the poles associated with the actuator dynamics become underdamped and move towards lower damping while the frequency stays roughly the same. Again, the more benign direction is an overastimation of the actuator time constant $\hat{T}$, since in this case the most significant pole merely moves towards lower frequencies while still being fully damped.

Finally, figure 4 shows a similar analysis for the effect of uncertainty in the time delay $\hat{\tau}$. As was already discussed in

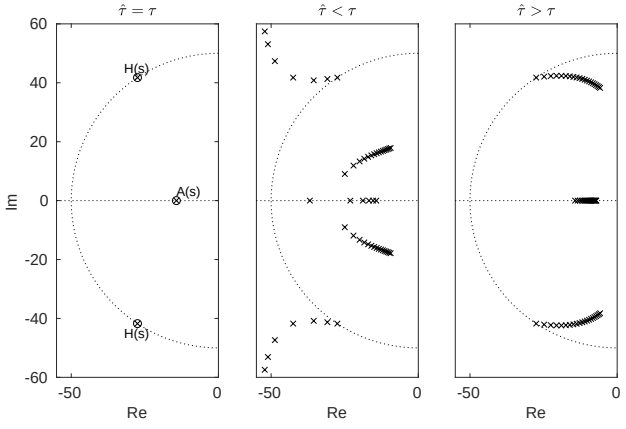

Figure 4: Effect of uncertainty in actuator delay on significant poles of INDI loop (sample time $T_s = 0.001$ sec), $\tau/T_s = 40, 0 < \hat{\tau}/T_s < 80$

the literature [1], a lack of assumed time delay $\hat{\tau}$ can lead to oscillations in the closed-loop. In case of underestimating the delay $\hat{\tau}$, the significant poles first tend towards faster dynamics, while still being fully damped. Once a critical error in the estimated delay $\hat{\tau}$ is reached, the dynamics become underdamped. The more benign case is again an overestimation of the delay $\hat{\tau}$, which leads to slower system dynamics. However, with an increasing overestimation of $\hat{\tau}$, the poles of the filter H become less damped and lead to visible oscillations in the time-domain response. Unfortunately, an error in the estimated delay leads to a behaviour, which is similar to the behaviour in case of an error in either the control effectivity M_u or the actuator time constant T. Determination of the delay τ can however be quite easily accomplished by either analyzing flight test data or performing dedicated testing of the actuators.

In summary, this analysis gives some insight into the behaviour of INDI in case of uncertainty. In our experience, a common problem when implementing INDI for a new aircraft are oscillations. Based on the discussion above, observing the frequency of the oscillations can give a hint as to what the source of the oscillations is. Appropriate mitigations can either be to adapt the assumed model $(\hat{M}_u, \hat{T}, \hat{\tau})$ accordingly or the parameters (ω_0, ζ) of the filter H. Additionally, overestimation of the control effectivity M_u and the actuator time constant T generally leads to slower dynamics and thus might serve as a good starting point for new controller designs. In section 4 we show how the performance of an INDI controller can easily be assesed and tuned in real-time, enabling rapid controller development.

3 Actuator Models

Small electric aircraft typically feature two kinds of actuators: rudders and electric motors with propellers to produce thrust. Depending on the configuration, the rudders might additionally be positioned in the slip-stream of the propellers. This configuration is often used to create rudder effectivity even when there is no aerodynamic velocity (e. g. flying-wings, tiltwing aircraft).

To model the effectivity of these actuators, we propose a two-step approach: First, we calculate the thrust, slip-stream velocity and effectivity of the motors. Second, we calculate the effectivity of the rudders, taking into acount slip-stream velocities if neccessary.

In addition to these *static* acutator model properties, we also model the *dynamic* behaviour of the actuators. This is of course only strictly necessary, when the actuator positions are not measured. Still, for designing the outer rate and attitude controllers, an estimate of the actuator dynamics is beneficial.

For both, the static and dynamic properties we rely as much as possible on properties which are either easily measurable or specified by the manufacturers. In Section 4 we analyze how well these actuator models actually perform and how this compares to the requirements on modeling fidelity derived in Section 2.

3.1 Static Actuator Effectivity Models

Within the scope of attitude control, the actuator effectivity describes the change in moments due to changes in actuator position (i. e. rudder deflection or throttle). For many applications it is sufficient to look at the force induced by an actuator and use the corresponding lever to calculate the induced moment. We thus get expressions of the form

$$\mathbf{M}_u = \frac{\partial \mathbf{M}}{\partial u} = \mathbf{r} \times \frac{\partial \mathbf{F}}{\partial u} \tag{4}$$

where $\mathbf{M}_u$ describes the actuator effectivity of an actuator u in the body-fixed coordinate frame given by the cross-product of the actuator position $\mathbf{r}$ and the induced change in force $\mathbf{F}$. In the following section we will mostly focus on determining the term $\partial \mathbf{F} / \partial u$.

3.1.1 Motors

The most common type of electric motor used in electric aircraft is the synchronous AC motor. It needs to be driven by a specialized electronic component called an Electronic Speed Controller (ESC), see Figure 5. An ESC is controlled via a throttle value δ, which can typically be normalized to ranges from 0 to 1 (or -1 to 1, if the ESC supports driving the motor in reverse). The ESC generates the appropriate voltages to drive the motor, resulting in an angular velocity measured as Revolutions Per Minute (RPM) n. Depending on the propeller and inflow conditions, these angular velocities then result in a thrust F. This description makes the simplifying assumption

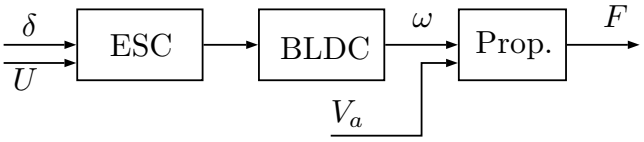

Figure 5: Motor model

that the angular velocity is independent of the inflow. It thus enables using a simpler model at the cost of modeling fidelity.

The motor model we propose consists of two parts: a mapping from the throttle δ and the supply voltage U of the ESC to the RPM n and a mapping from n combined with the inflow V_a to the thrust F.

ESC/BLDC model When the motor RPMs are not measured, we use the following model based on the supply voltage U, the motor speed constant K_V and the throttle setting δ

$$n = U \cdot K_V \cdot \delta \tag{5}$$

This model basically assumes that the motor is in a no-load condition, which is a very crude approximation. The advantage is however, that only the parameter K_V needs to be known, which is usually specified by the motor manufacturer.

Propeller Model For small electric aircraft a database of measured propeller performance exists [9]. Also some manufacturers provide additional performance preditictions [10] based on analytical methods. To model the propeller thrust we first calculate the static thrust produced at zero inflow speed and then correct this value using an estimate of the current inflow speed. We model the static thrust as

$$T_1 = K_1 n^2 \tag{6}$$

The value of K_1 can either be derived using one of the previously mentioned propeller databases, from simple test setups or from previously acquired flight data.

To correct for the inflow velocity, we add a correction term, resulting in

$$T = K_1 n^2 + K_2 V n \tag{7}$$

where V represents the axial inflow speed. The actuator effectivity according to (4) thus becomes

$$T_n = \frac{\partial T}{\partial n} = 2K_1 n + K_2 V \tag{8}$$

This choice of correction term is informed by the propeller data displayed in Figure 6. Figure 6 shows the thrust produced by a propeller[1] at different axial velocities and at different RPMs. For the relevant inflow speeds ($< 20\,\mathrm{m\,s^{-1}}$) and the

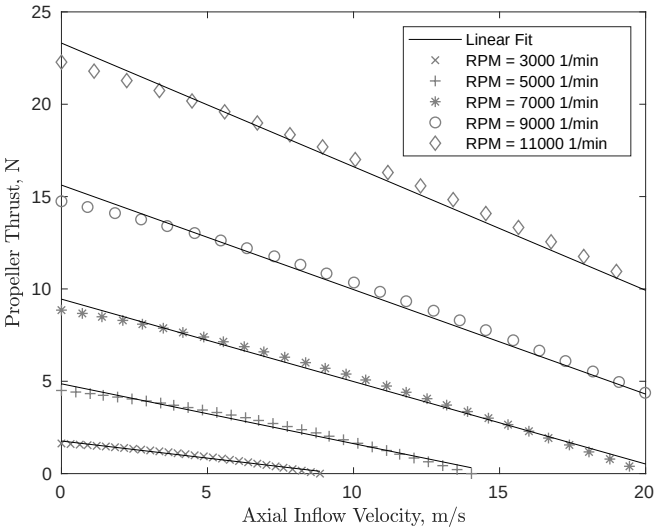

Figure 6: Thrust over axial velocity

region of relevant RPMs an affine function approximates the data well. Given these data, K_1 and K_2 can be found by fitting the propeller model (7) to the data. If propeller data are not available K_2 can be calculated using analytical approaches like blade element momentum theory [11].

As a first approximation, K_2 can also be interpolated from available propeller performance data. The performance database published in [10] was calculated using blade element momentum theory. While here the parameter K_1 is consistently overestimated, the parameter K_2 matches the measured data published in [9] well. The data suggest that K_2 can be approximated as a function of the propeller diameter D and the propeller pitch S:

$$K_2 = p_{11} D^2 + p_{10} D + p_{20} S + p_0 \tag{9}$$

Fitting this function over the available data results in the following model parameters (all units in inch, if applicable):

Database	p_{11}	p_{10}	p_{20}	p_0
UIUC [9]	-1.79e-06	1.70e-05	2.30e-06	-6.75e-05
APC [10]	-1.75e-06	1.70e-05	8.51e-06	-9.28e-05

Since the UIUC database [9] features a wide range of different propeller types and manufacturers, we expect that the corresponding model will extrapolate well to new propellers.

3.1.2 Rudders

We approximate rudders as thin plates, where the rudder effectivity is given by

$$F_\delta = \frac{\partial F}{\partial \delta} = 2\pi \cdot \frac{\rho}{2} V^2 S \cdot \frac{\Lambda}{\Lambda + 2} \tag{10}$$

with the air density ρ, inflow speed V, rudder aera S and aspect ratio Λ. If a rudder is partly in the slip stream of a propeller, the rudder is split accordingly into separate parts. In this case, the aspect ratio Λ still represents the aspect ratio of the whole rudder. The inflow speed V is either the free stream speed or the slip stream speed. In the latter case, we apply momentum theory and assume that the slip stream is fully developed. [5] shows a more detailed example of this approach. Using the propeller model (7) to calculate the thrust T produced by the corresponding propeller, this gives the slip stream velocity as

$$V = \sqrt{\frac{T}{S}\frac{2}{\rho} + V_A^2} \tag{11}$$

where V_A is the inflow speed of the propeller, usually the measured airspeed.

3.2 Dynamic Actuator Models

For dynamic actuator models we use first-order lags with time-delay and optional rate-limit, which is a common approach found in the literature [3, 4]. Figure 7 shows the corresponding block diagram. The actuator time constant T and the rate limit (denoted as $\dot{\theta}_{\max}$) can either be measured or approximated using the manufacturers specifications. Typically, we only model servo motors with a rate limit.

[1] APC 10x3.8 Slow Fly

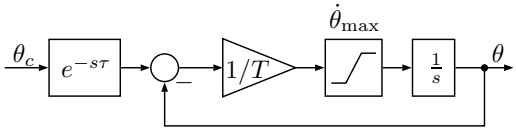

Figure 7: Actuator Model

4 Analysis

In this section we analyze the accuracy of the previously described models. Where possible, we validate the models using measured data from flight tests or other test setups. We already presented the rudder model presented here in previous work [5]. Determining the fidelity of the model would require dedicated wind-tunnel testing which was beyond the scope of this work. We thus don't discuss the rudder effectivity model further in the following analysis.

4.1 Motor model

The motor model consists of two parts: the ESC/BLDC model and the propeller model. To validate the ESC/BLDC model, we analyzed flight test data of a tiltwing aircraft, where the RPM were measured. Figure 8 shows a comparison of the predicted RPM and the measured RPM. As mentioned previously, the ESC/BLDC model assumes a no-load condition, which naturally does not reflect the actual flight conditions. Thus, using the K_V value specified by the manuafacturer will always result in an overestimation of the RPM. The relative error between the expected RPM $\hat{n}$ and the measured RPM n is about $20\,\%$. We found similar accuracies when analyzing wind-tunnel measurement data. The model can be significantly improved by adjusting (i. e. lowering) the K_V value to account for the additional load-conditions. However, implementing such an adjustment requires measuring the actual RPM, in which case the ESC/BLDC model is not needed anyways. Thus, we recommend using the manufacturers K_V value, if RPM measurements are not available. Note, that this model fails to represent fast decelerations, because in this case the propellers are in a windmilling state and are accelerated by the inflow, which is not represented in the model.

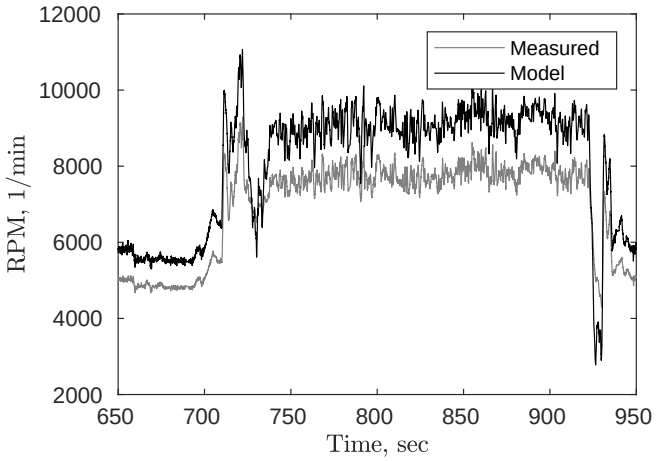

Figure 8: BLDC/ESC model

The propeller model (8) consists of two constants K_1 and K_2. We assume that K_1 can be accurately determined from the static motor model (6). K_2 however has to be either measured in wind-tunnel tests or determined using analytical methods. The approximation of K_2 as a function of the propeller diameter and propeller pitch given in (9) can be used as a first approximation if no other data are available. It is however not clear if over- or underestimation occurs. In our experience, K_2 only becomes significant at high airspeeds, at which point the rudder effectivity usually is high enough for the rudders to act as the primary control surface.

In summary, we expect the motor model to be sufficiently accurate with a tendency to overestimate the propeller effectivity. Thus, reffering to Figure 2, this should result in fully damped system dynamics.

4.2 Dynamic actuator model

The rate-limited first-order lag model used to model servo motors has three parameters: the rate limit $\dot{\theta}_{\max}$, the time constant T and the delay τ. Typically, servo manufacturers only specify a "servo speed" given as the time needed to travel a certain angular distance. Unfortunately it is not clear how exactly this speed specification relates to the servo parameters given above. Directly using the servo speed as the rate limit does certainly not result in an accurate model. To find the model parameters, dedicated tests have to be conducted, for example by probing the internal potentiometer output of the servo motor as suggested in [4]. As an alternative, we built a servo testbench, which also permits us to study the frequency-dependent behaviour of a servo motor. Figure 9 shows the commanded angle and the measured servo angle over time. As is clearly visible, the servo motor cannot reach the commanded amplitude at this frequency. The rate-limit thus leads to an attenuation of the input signal. There is also a phase delay between the commanded and the actual signal. The attenuation and the phase delay give rise to a Bode plot, where we define the phase shift as the value which provides the best-fit between input and output signal.

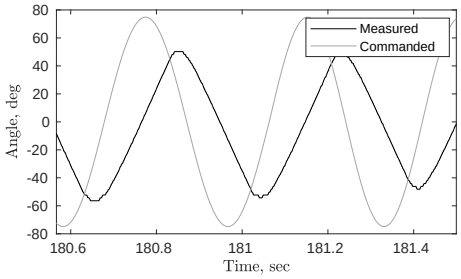

Figure 9: Servo dynamics at high frequencies

Figure 10 shows an example Bode plot obtained by running the test displayed in Figure 9 for many different frequencies. It is clear, that a low-order linear servo model cannot capture the magnitude and phase behaviour of the nonlinear servo model. The sharp edge in the magnitude plot is related to the nonlinear effects of the rate limit. The time constant T of the servo actually has little impact on the overall modeling accuracy. How and if this actuator model should influence the

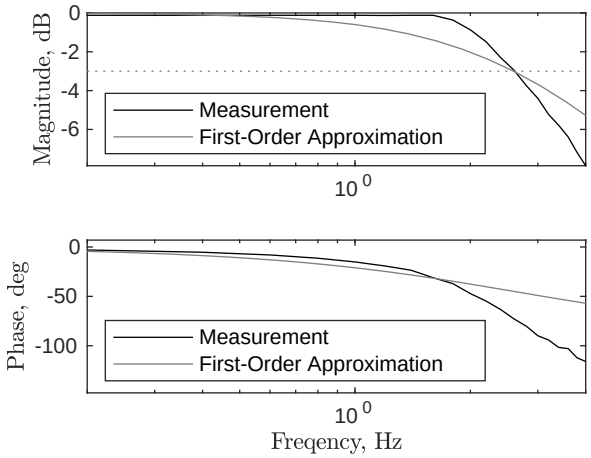

Figure 10: Bode plot of servo dynamics

design of outer loop controllers still needs to be investigated. As a comparison, Figure 10 also shows an approximation of the nonlinear servo model using a first-order lag, where the time constant is chosen such that it matches the edge frequency of the nonlinear servo model. In terms of designing outer loop controllers, such an approximation might serve as a useful abstraction of the nonlinear dynamic model to still allow the application of linear control methods.

In summary, the actuator models presented here are able to capture the dynamic behaviour of the real actuators well. In case of electric motors, simple linear models seem to sufficiently capture the relevant dynamics. In the case of servo motors, the model parameters are hard to derive based on the typical manufacturer specifications. To apply the analysis summarized in Figure 3 suitable alternative (linear) actuator models need to be derived.

5 Conclusion

This paper presented our approach to modeling actuators for use in the framework of INDI. First, by studying the effects of modeling uncertainty on the poles of the closed-loop system, the robustness properties of INDI controllers were analyzed. We confirmed the known stability properties of INDI, but found that the uncertainty bounds of acceptable closed-loop performance are (of course) much tighter. With that in mind, we then considered the typical actuator elements found in small electric aircraft, namely electric motors with propellers and rudders actuated by servo motors. We derived suitable models for these elements, trying to rely as much as possible and easily obtainable information.

In the following analysis we assessed the resulting model fidelity using real flight data or measurements where possible. Special consideration was given to typical servo models, which feature a nonlinear rate-limit element. We discussed some effects of this nonlinearity, though further works needs to investigate how and if these nonlinearities should be considered in the design of outer loop controllers.

References

[1] R C van't Veld, E van Kampen, and Q P Chu. Stability and Robustness Analysis and Improvements for Incremental Nonlinear Dynamic Inversion Control. (January), 2018.

[2] S Sieberling, Q P Chu, and J A Mulder. Robust Flight Control Using Incremental Nonlinear Dynamic Inversion and Angular Acceleration Prediction. *Journal of Guidance, Control, and Dynamics*, 33(6):1732–1742, 2010.

[3] Ewoud J J Smeur, Qiping Chu, and Guido C H E de Croon. Adaptive Incremental Nonlinear Dynamic Inversion for Attitude Control of Micro Air Vehicles. *Journal of Guidance, Control, and Dynamics*, 39(3):450–461, 2016.

[4] Murat Bronz, Ewoud J Smeur, Hector Garciade de Marina, and Gautier Hattenberger. Development of A Fixed-Wing mini UAV with Transitioning Flight Capability. In *AIAA Applied Aerodynamics Conference, Aviation Forum, At Denver, Colorado*, 2017.

[5] Fabian Binz, Tobias Islam, and Dieter Moormann. Attitude Control of Tiltwing Aircraft Using a Wing-Fixed Coordinate System and Incremental Nonlinear Dynamic Inversion. In *10th International Micro Air Vehicle Competition and Conference*, pages 86 – 93, 2018.

[6] Barton J Bacon and Aaron J Ostroff. Reconfigurable Flight Control using Nonlinear Dynamic Inversion with a Special Accelerometer Implementation. In *AIAA Guidance, Navigation, and Control Conference and Exhibit*, number August, 2000.

[7] Fabian Binz, Philipp Hartmann, and Dieter Moormann. Nonlinear Model Predictive Flight Path Control for an Unmanned Powered Paraglider. In *Euro GNC 2017 - 4th CEAS Specialist Conference on Guidance, Navigation & Control*, 2017.

[8] E J J Smeur, G C H E De Croon, and Q Chu. Cascaded incremental nonlinear dynamic inversion for MAV disturbance rejection. *Control Engineering Practice*, 73(January):79–90, 2018.

[9] J.B. Brandt, R.W. Deters, G.K. Ananda, and M.S. Selig. UIUC Propeller Database, 2019.

[10] APC Propeller Performance Data.

[11] Matthew H McCrink and James W Gregory. Blade Element Momentum Modeling of Low-Re Small UAS Electric Propulsion Systems. *AIAA Aviation*, (June):1–23, 2015.